2013-09-13

Channelized Ice Melting in the Ocean Boundary Layer Beneath Pine Island Glacier, Antarctica

Stanton, Timothy P.; Shaw, W.J.; Truffer, M.; Corr, H.F.J.; Peters, L.E.; Riverman, K.L.; Bindschadler, R.; Holland, D.M.; Anandakrishnan, S.

Science 341 (September 2013), p. 1236-1239
https://hdl.handle.net/10945/48294

Channelized Ice Melting in the Ocean Boundary Layer Beneath Pine Island Glacier, Antarctica

T. P. Stanton,[1]* W. J. Shaw,[1] M. Truffer,[2] H. F. J. Corr,[3] L. E. Peters,[4] K. L. Riverman,[4] R. Bindschadler,[5] D. M. Holland,[6] S. Anandakrishnan[4]

Ice shelves play a key role in the mass balance of the Antarctic ice sheets by buttressing their seaward-flowing outlet glaciers; however, they are exposed to the underlying ocean and may weaken if ocean thermal forcing increases. An expedition to the ice shelf of the remote Pine Island Glacier, a major outlet of the West Antarctic Ice Sheet that has rapidly thinned and accelerated in recent decades, has been completed. Observations from geophysical surveys and long-term oceanographic instruments deployed down bore holes into the ocean cavity reveal a buoyancy-driven boundary layer within a basal channel that melts the channel apex by 0.06 meter per day, with near-zero melt rates along the flanks of the channel. A complex pattern of such channels is visible throughout the Pine Island Glacier shelf.

In a state of equilibrium, the Antarctic Ice Sheet loses mass through the melting and calving of its outlet glaciers at the same rate as it gains mass through the accumulation of snowfall. Ice shelves, the floating portions of outlet glaciers, provide a control on this equilibrium through a buttressing effect, in which the lateral friction of the ice shelf side walls impedes ice flow, allowing additional ice mass to accumulate upstream of the ice shelf. If ice shelves melt rapidly or break away, equilibrium is lost, ice flow accelerates, and ice sheets experience a net mass loss.

Currently, ice loss from the Amundsen Sea sector of the West Antarctic Ice Sheet (WAIS) contributes ~7% of the global sea-level rise. The WAIS is potentially dynamically unstable, with a capacity to raise global sea level by several meters (*1*). Pine Island Glacier (PIG) is a principal outlet of the WAIS that has rapidly thinned, retreated, and accelerated (*2*–*6*). The spatial pattern of thinning suggests that the glacier drawdown is the direct result of increased basal melting of the ice shelf that has reduced its buttressing effect. The restraint offered by the PIG ice shelf is dependent on its basal melt rate, which in turn is controlled by heat transport in the underlying ocean cavity. Therefore, how an ice shelf interacts with the ocean and melts now and into the future can alter the mass discharge from the Antarctic Ice Sheet in general and the WAIS in particular, affecting global sea level.

The inaccessibility of ice shelf ocean cavities, which are overlain by glacial ice hundreds of meters thick, and the Amundsen Sea ice shelves, which are thousands of kilometers distant from established Antarctic research stations, has severely limited attempts to directly observe ice shelf/ocean interactions in this sector. Successful icebreaker cruises into Pine Island Bay in 1994 and 2009 surveyed hydrography and deployed long-term moorings along the PIG terminus (*7*, *8*). The 2009 cruise included six runs of the unmanned submersible Autosub under the shelf (*9*). These data sets show relatively warm Circumpolar Deep Water (CDW) intruding up onto the continental shelf to the PIG terminus, and 30 km into the ocean cavity. Between 1994 and 2009, the water column became warmer and saltier, and meltwater volume estimates increased by 50%, driven primarily by increased circulation rather than increased heat content (*8*). For 2009, the hydrography-based estimate of mean shelfwide basal melt rate was 33 m year^{-1} (*8*)

The Autosub missions and a dense airborne ice-penetrating radar survey (*10*) have characterized aspects of the ice shelf morphology and ocean cavity bathymetry. Autosub altimeter data revealed a 300-m-high, 700-m-deep transverse ridge that effectively splits the ocean cavity into inner and outer cavities. The airborne radar sections revealed

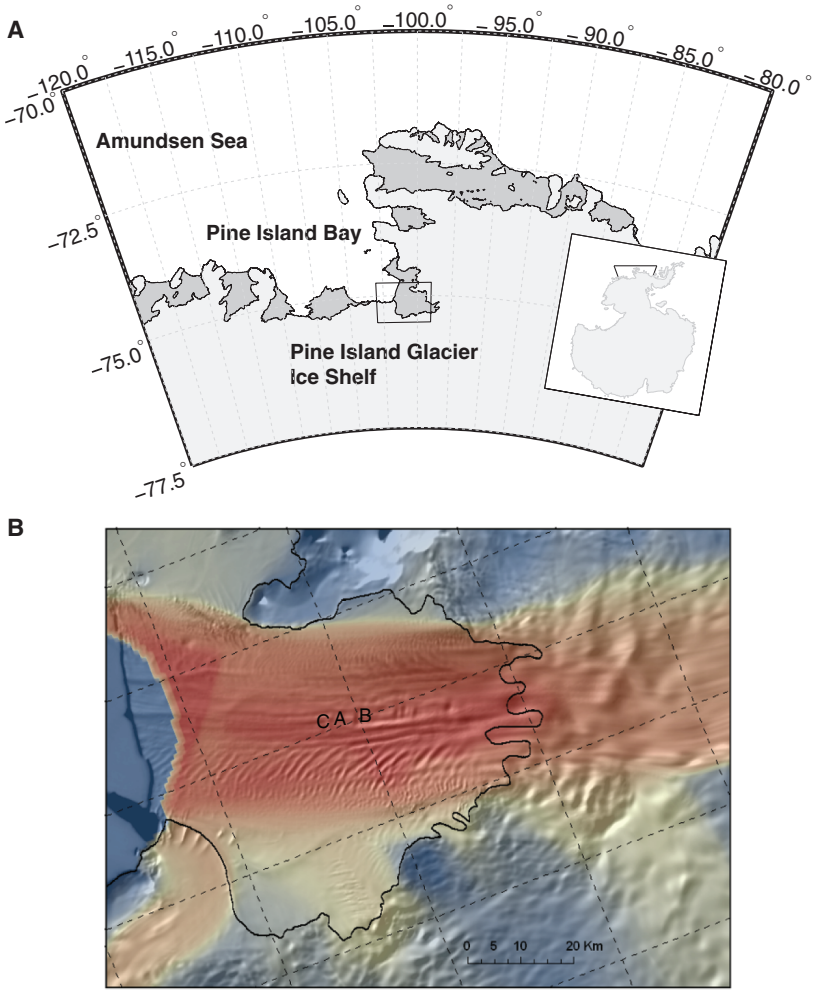

Fig. 1. Locations of the 2012/2013 Pine Island Ice Shelf drill camps. (**A**) Map showing the Amundsen Sea and Pine Island Bay. Light gray is the continental ice sheet; darker gray shows ice shelf areas. The inset map in the lower right shows the entire Antarctic continent, and the smaller box in the lower center shows the PIG area, expanded on in (B). (**B**) A composite of surface satellite imagery (*15*) overlaid with satellite-derived ice surface velocity (*16*) with blue indicating 0 m s^{-1} and red indicating 4000 m s^{-1}. An estimate of the grounding line location is shown as a black line (*17*). The three drill camp locations are shown as A, B, and C.

[1]Department of Oceanography, Naval Postgraduate School, Monterey, CA 93943, USA. [2]Geophysical Institute, University of Alaska, Fairbanks, AK 99775–7320, USA. [3]British Antarctic Survey, Cambridge, CB3OET, UK. [4]Department of Geosciences and Earth and Environmental Systems Institute, The Pennsylvania State University, University Park, PA 16802–2711, USA. [5]Emeritus Scientist, NASA Goddard Space Flight Center, Greenbelt, MD 20771, USA. [6]Department of Mathematics, New York University, NY 10012, USA.

*Corresponding author. E-mail: stanton@nps.edu

a network of longitudinal subshelf channels 0.5 to 3 km wide, with basal crevassing confined to the center of the channels. Extensive surface crevassing was observed along the tops of each of these ridges, indicating lateral tension driven by local hydrostatic imbalance between adjacent ridges and troughs (*11*).

Here we report on a dynamical view of basal melting and the ocean boundary layer below PIG, obtained from surface geophysical surveys and in situ observations within one of the PIG subshelf channel systems. To obtain these observations a (relatively) lightweight hot-water drilling rig, that could be transported by light aircraft and snow machines, was used to make 20-cm-diameter holes through the 400- to 500-m-thick ice shelf. A specialized suite of ocean instrumentation was developed that could fit down the narrow holes, sample turbulence and lateral transport rates in the ocean cavity, and autonomously offer two-way communication of data and sampling commands over year-long sampling periods. These detailed observations are required to understand the physical processes in the ocean cavity, and their variability, that control basal melting.

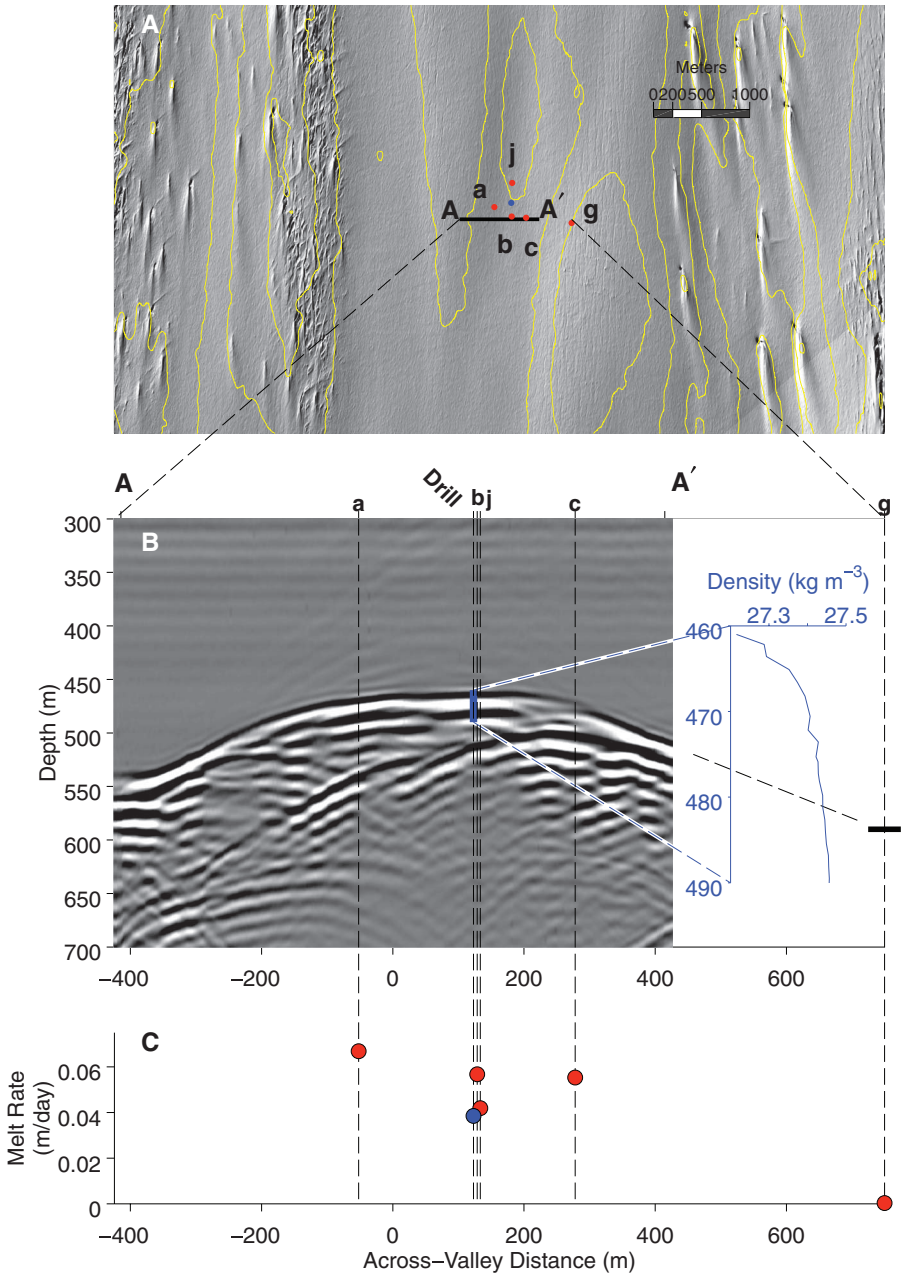

Fig. 2. Ice shelf surface and basal structure, and basal melt rates. (**A**) 1-m-resolution visible satellite image of the area around drill A with a 5-MHz ice-penetrating radar transect shown as the A–A′ line. pRES sites are a, b, c, j, and g. (**B**) An upstream-looking channel cross-section from the radar transect. The ice bottom is visible from 450 to 550 m, referenced from the ice surface. A CTD density anomaly profile between 460 and 490 m shown on the right indicates the structure 30 m down through the buoyant ocean boundary layer plume. (**C**) pRES melt rates for the five locations in (**A**) are shown as red dots, with the scale in red on the right. The blue bar and dot represent 35-day mean melt rates from the flux package altimeter deployed from the bore hole.

Three drilling camps (Drill A, B, and C) were established on the PIG shelf during December 2012 and January 2013 to access the ocean cavity. The camps were positioned in the center of the shelf, away from the heavily crevassed side shear zones (Fig. 1B) and within an approximately 1-km transverse wavelength valley and ridge system observed in previous airborne radar surveys (*10*) (Fig. 2A). This shallow, snowdrift-covered valley is flanked by crevassed ridges, with ridge-to-valley surface elevation changes on the order of 10 m (*O*). Drills A and C were seaward of the transverse seafloor ridge, and Drill B was located on the up-glacier side of the ridge. Here we focus on Drill A observations.

An 850-m-long across-valley transect was made with low-frequency radar (Fig. 2A). Basal melt rates near the radar transect line were measured using a phase-coherent radar (pRES) at five sites (referred to as pRES a, b, j, c, and g; see methods in the supplementary materials). The drilling of a 450-m-deep hole through the ice shelf permitted a full water column conductivity-temperature-depth (CTD) cast and the deployment of a long-term, fixed-depth "flux package." The flux package, initially deployed with its sample volume 2.3 m below the ice, tracks the ice/ocean interface with an altimeter and measures ocean velocity, temperature, and salinity at a sufficiently fast rate (4 Hz) to calculate vertical turbulent fluxes of momentum, heat, and salt.

The radar echogram (Fig. 2B) shows a 600-m-wide, smooth-sided basal channel, with ice shelf thickness on the underside of the shelf decreasing from 540 m on the channel banks to 460 m near the center. At pRES b and j, melt rates of 0.0570 ± 0.0003 m day^{-1} and 0.0420 ± 0.0003 m day^{-1} were determined from continuous time series of length 29.4 and 14.6 hours. At pRES a and c, melt rates of 0.067 m day^{-1} and 0.055 m day^{-1} were calculated by reoccupying the sites at 11- and 13-day intervals, respectively. At pRES g, on the channel bank, basal melting was <0.001 m day^{-1}, near the resolution limit of the system (Fig. 2B). Flux package acoustic backscatter profiles precisely track the ice/ocean interface (Fig. 3A). Melting within the *O* (5 cm) altimeter footprint (Fig. 3B) is fairly steady, with a linear fit from day 5 to 35 yielding a rate of 0.039 m day^{-1}. The altimeter melt rate is nearly equal to the adjacent pRES j rate, whereas it is 30% less than the pRES b rate, located 80 m upstream from the drill hole. Taken together, the melt rate estimates show that, at Drill A, there is rapid, spatially uniform, and steady basal melting within the channel and minimal melting outside of the channel (Fig. 2C).

Time series of Reynolds-averaged ocean properties show that the channel boundary layer was relatively warm and fresh and steady over the month when these observations were collected.

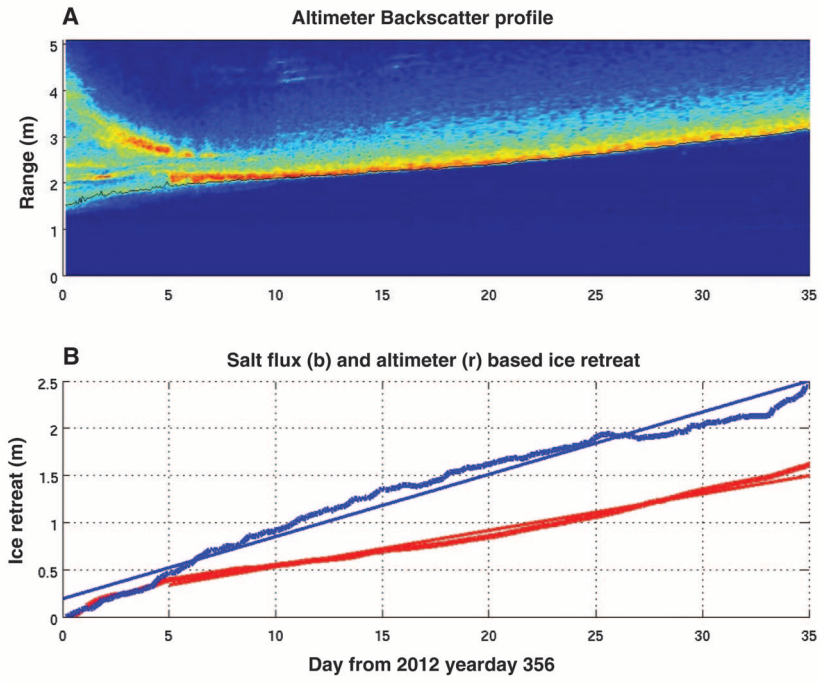

Fig. 3. Time series of the ocean/ice interface retreat. (**A**) 35-day time series starting at 22 December 2012 of acoustic backscatter strength from an upward-directed altimeter on the fixed-position flux package. The blue-to-red color scale represents a five order of magnitude change in backscatter strength. The derived ice/ocean interface is traced as a thin black line. (**B**) The thick red line represents the backscatter-inferred interface, whereas the thinner red line is a linear fit from days 5 to 35. The thick blue line is an ice retreat estimated from temporally integrated turbulent salt fluxes measured by the flux package, whereas the thin blue line is the corresponding linear fit to this retreat rate.

Mean current speed (Fig. 4A) increased uniformly from 0.11 to 0.15 m s^{-1}, whereas the mean current direction was consistently seaward, along the channel axis (not shown in Fig. 4). There were no tidal or other distinct oscillatory motions in the boundary layer fluctuations over the 35-day period considered here. Departure from freezing increased uniformly from 1.35 to 1.42 K (Fig. 4C). Most likely, these gradual changes in measured mean current speed and temperature are the result of vertical gradients within the strongly sheared boundary layer moving past the sensors as the ice/ocean interface slowly receded. Near-interface salinity was 33.85 practical salinity units (psu), which is fresher than the 34.1-psu surface waters observed in terminus surface waters in 2009 (*7*). The turbulent shear stress was steady, with a mean friction speed of 0.0086 m s^{-1} (Fig. 4B, methods, and eq. S1). Vertical salt fluxes were variable, including negative values, with a 35-day mean value of 2.8×10^6 psu m s^{-1}. Positive salt fluxes represent downward turbulent fluxes of fresh water from melting at the ice shelf base.

Integration of the vertical salinity flux provides a history of interface retreat (Fig. 3B, methods, and eq. S2) that is an areal average of upstream melting and so is potentially more representative than the altimeter-based estimate. The average melt rate inferred from the salt flux is 0.066 m day^{-1}. This flux-based melt rate estimate agrees well with the pRES and altimeter estimates, connecting the basal melting of the ice shelf to turbulence in the channelized ocean boundary layer.

The CTD density profile (Fig. 2B) shows that the boundary layer is thin (12 m) and buoyant. The basic dynamics of the layer were examined by testing a simplified, vertically integrated momentum balance (*12*), in which the buoyancy force

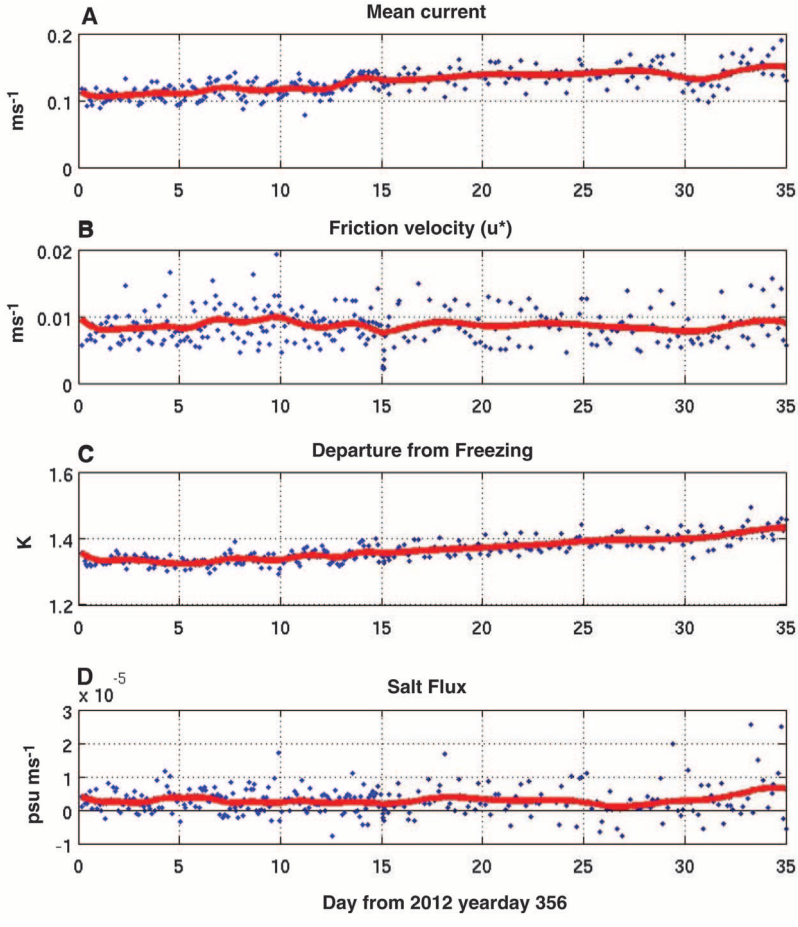

Fig. 4. Time series of ocean boundary layer properties. A corresponding time series of mean current (**A**), turbulent friction velocity (**B**), the departure from freezing $T_d = T - T_{fp}$ (T, in situ temperature; fp, the pressure- and salinity-dependent local freezing point) (**C**), and turbulent vertical salt flux (**D**) from the fixed position turbulent flux package at Drill A with the same time axis as Fig. 3. The thick red lines represent 2-day-period low-pass filtered versions of each time series.

arising from the vertical density gradient and the sloping interface

$$\alpha g \int_0^{\delta} (\rho - \rho_\delta) dz \quad (1)$$

is balanced by the turbulent shear stress at the interface. With density ρ and layer height δ taken from the CTD profile and basal slope α calculated from depth differences between Drill A and B, the buoyancy force is estimated at 0.043 Pa. This compares favorably to the average shear stress measured by the flux package, $\rho u_*^2 =$ 0.076 Pa (Fig. 4B), indicating that the observed boundary layer flow is forced by the melt-generated buoyancy acting along the sloping base of the shelf.

These in situ measurements of the underside of the PIG ice shelf reveal strong but spatially non-uniform ice/ocean interaction, in which ocean boundary layers are strongly coupled to basal melting: They are buoyantly forced by melt water and are constrained by the resulting melt channel morphology. The pRES melt rate estimates document the cross-channel variability in melt rate that results from the channelized flow, whereas the longer-term flux package estimates demonstrate that melt rates and boundary layer properties were fairly steady over the month of observations, which is consistent with the idea that the forcing is due to the relatively slowly evolving buoyancy field within the ocean cavity. If these direct melt rates within the channel are annualized, they range between 14.2 and 24.5 m $year^{-1}$. However, we expect that melt rates will be affected by seasonal or other long–time-scale variability associated with the oceanic forcing. We also expect along-shelf spatial variability in cross-shelf melt patterns, as supported by recent altimetry analyses (*13*) that infer preferential melting of keels toward the terminus. The continuity of the channels seen in satellite imagery and the airborne radar survey, in conjunction with the vigorous melt rates here described, indicate that basal melting is active from the grounding line to at least the mid-shelf location of the observations. In addition to our observations, a recent idealized numerical simulation of an ice shelf base and ocean boundary layer has suggested that channelization is of fundamental importance, because a channelized base actually melts much less vigorously than a nonchannelized one (*14*). The remarkable ice/ocean coupling evident in our observations points to the need to represent channelized ice/ocean interaction in models of PIG and similar outlet glaciers in global climate simulations of sea-level change.

References and Notes

1. J. L. Bamber, R. E. M. Riva, B. L. Vermeersen, A. M. LeBrocq, *Science* **324**, 901–903 (2009).
2. E. Rignot *et al*., *Nat. Geosci.* **1**, 106–110 (2008).
3. A. Shepherd, D. J. Wingham, J. A. D. Mansley, H. F. J. Corr, *Science* **291**, 862–864 (2001).
4. D. J. Wingham, D. W. Wallis, A. Shepherd, *Geophys. Res. Lett.* **36**, L17501 (2009).
5. A. J. Payne, A. Vieli, A. P. Shepherd, D. J. Wingham, E. Rignot, *Geophys. Res. Lett.* **31**, L23401 (2004).
6. H. D. Pritchard, R. J. Arthern, D. G. Vaughan, L. A. Edwards, *Nature* **461**, 971–975 (2009).
7. S. S. Jacobs, H. H. Hellmer, A. Jenkins, *Geophys. Res. Lett.* **23**, 957–960 (1996).
8. S. S. Jacobs, A. Jenkins, C. F. Giulivi, P. Dutrieux, *Nat. Geosci.* **4**, 519–523 (2011).
9. A. Jenkins *et al*., *Nat. Geosci.* **3**, 468–472 (2010).
10. D. G. Vaughan *et al*., *J. Geophys. Res.* **117**, F03012 (2012).
11. R. Bindschadler, D. G. Vaughan, P. Vornberger, *J. Glaciol.* **57**, 581–595 (2011).
12. J. H. Trowbridge, S. J. Lentz, *J. Phys. Oceanogr.* **28**, 2075–2093 (1998).
13. P. Dutrieux *et al*., *Cryosphere Discuss* **7**, 1591–1620 (2013).
14. C. V. Gladish, D. M. Holland, P. R. Holland, S. F. Price, *J. Glaciol.* **58**, 1227–1244 (2012).
15. T. Haran, J. Bohlander, T. Scambos, T. Painter, M. Fahnestock, compilers, *Moderate Resolution Imaging Spectroradiometer (MODIS) Mosaic of Antarctica (MOA) Image Map* (National Snow and Ice Data Center, Boulder, CO, 2005, updated 2006) (digital media).
16. E. Rignot, J. Mouginot, B. Scheuchl, *Science* **333**, 1427–1430 (2011).
17. R. Bindschadler *et al*., *Cryosphere* **5**, 569–588 (2011).

Acknowledgments: Data presented here are archived with the supplementary materials and also as a MATLAB data structure at www.oc.nps.edu/~stanton/pig/data/data.html/PIGSITE1_first35days. The authors acknowledge the contributions of J. Stockel in software development and deployment of the ocean instruments, D. Pomraning in designing and manning the hot-water drill equipment, and M. Shortt for making the British Antarctic Survey pRES field measurements. Outstanding logistic and safety support was provided by K. Gibbon, D. Einerson, E. Steinarsson, F. Mcarthy, S. Consalvi, the PIG support camp personnel, and the NSF Antarctic support team. This research project was supported by NSF's Office of Polar Programs under NSF grants including ANT-0732926, funding from NASA's Cryospheric Sciences Program, New York University Abhu Dabi grant 1204, and the Natural Environment Research Council–British Antarctic Survey Polar Science for Planet Earth Program.

Supplementary Materials

www.sciencemag.org/cgi/content/full/341/6151/1236/DC1
Materials and Methods
References (*18*–*21*)

19 April 2013; accepted 6 August 2013
10.1126/science.1239373

Marine Taxa Track Local Climate Velocities

Malin L. Pinsky,[1,2]* Boris Worm,[3] Michael J. Fogarty,[4] Jorge L. Sarmiento,[5] Simon A. Levin[1]

Organisms are expected to adapt or move in response to climate change, but observed distribution shifts span a wide range of directions and rates. Explanations often emphasize biological distinctions among species, but general mechanisms have been elusive. We tested an alternative hypothesis: that differences in climate velocity—the rate and direction that climate shifts across the landscape—can explain observed species shifts. We compiled a database of coastal surveys around North America from 1968 to 2011, sampling 128 million individuals across 360 marine taxa. Climate velocity explained the magnitude and direction of shifts in latitude and depth much more effectively than did species characteristics. Our results demonstrate that marine species shift at different rates and directions because they closely track the complex mosaic of local climate velocities.

Global warming during the past century has had many biological effects, including changes in phenology and poleward shifts in species distributions (*1*–*3*). However, species have not responded uniformly, and shifts in their distributions have occurred at widely different rates and in different directions (*1*–*10*). In both marine and terrestrial assemblages, up to 60% of species are not shifting as expected; i.e., to higher latitudes, higher elevations, or greater depths (*1*–*10*). A range of hypotheses has been proposed to explain this observed variation, including the effects of habitats (*11*), species interactions (*11*, *12*), sensitivity to environmental gradients (*13*), response times (*10*), colonization abilities (*14*), and physiological or evolutionary adaptations (*15*). In essence, many of the leading hypotheses have emphasized biological differences among species (*8*–*10*, *14*).

An alternative and possibly more general hypothesis posits that local differences in climate velocity (*16*, *17*) can explain heterogeneity in species shifts. Climate velocity is the rate and direction that isotherms shift through space, and it combines both temporal and spatial rates of temperature change (*16*, *17*). Previous authors have hypothesized that species may follow

[1]Department of Ecology and Evolutionary Biology, Princeton University, Princeton, NJ 08544, USA. [2]Department of Ecology, Evolution, and Natural Resources and the Institute of Marine and Coastal Sciences, Rutgers University, New Brunswick, NJ 08901, USA. [3]Department of Biology, Dalhousie University, Halifax, NS B3H 4R2, Canada. [4]Northeast Fisheries Science Center, Woods Hole, MA 02453, USA. [5]Atmospheric and Oceanic Sciences Program, Princeton University, Princeton, NJ 08544, USA.

*Corresponding author. E-mail: malin.pinsky@rutgers.edu